Research On Photovoltaic Grid-Connected Inverter Based On Soft-Switching Interleaved Flyback Converter

GU Jun-yin
School of Electromechanical Engineering and Automation
Shanghai University
Shanghai, China
junyin_gu@yahoo.com.cn

WU Hong-fei
College of Automation and Engineering
Nanjing University of Aeronautics and Astronautics
Nanjing, China
wuhongfei@nuaa.edu.cn

CHEN Guo-cheng
School of Electromechanical Engineering and Automation
Shanghai University
Shanghai, China
gchchen@mail.shu.edu.cn

XING Yan
College of Automation and Engineering
Nanjing University of Aeronautics and Astronautics
Nanjing, China
xingyan@nuaa.edu.cn

***Abstract*—A grid-connected photovoltaic inverter based on interleaved flyback converter and a novel control strategy with BCM and soft switching are proposed in this paper. Power rating of the inverter can be dramatically increased due to the fact that the peak rated power of each of N interleaved flyback converter is 2/N of the total rated power. In order to increase the efficiency of the converter by eliminating the impact of leak inductance of the flyback transformer, inherited from the low voltage input and high voltage output applications, a leak inductance energy recovery circuit is proposed to restore the leak inductance energy and to achieve active clamping and resonant ZVS of the main switch at the same time. It is therefore possible to use flyback converters in higher power rating applications, as the N interleaved converters share the same leak inductance energy recovery circuit. In-depth analysis is presented on overall principal, variable switching frequency BCM and resonant ZVS with experimental results given. The proposed converter exhibits satisfactory character of high efficiency, simple topology, robust control and high reliability.**

Keywords-flyback converter; grid-connected PV; soft switching; inverter

I. INTRODUCTION

The interest in natural energy sources has been great increased for growing concerns for the environment. Many kinds of inverter circuits and corresponding control schemes for photovoltaic power generation systems have been studied [1]. Since the implantation of large-scale PV power plants is not cost-effective in urban applications like BIPV and roof-top, decentralized grid-connected PV systems are gaining more and more recognition as they can be easily installed as well as achieving individual MPPT yielding in more energy harvest[2].

It has been proven that flyback converters show the characteristics of current source when working in DCM (Discontinuous Current Mode) or BCM (Boundary Current Mode) [3]. Therefore, grid-tied applications can be achieved with PLL (Phase Locked Loop) alone and closed loop current control can be avoided for easy implementation and reduction of cost. Based on the flyback converter, many topologies, named as flyback inverter, have been proposed for the photovoltaic grid-connected application [4-12]. In those proposed topologies, the flyback inverter works alternatively in every half grid cycle and the maximum power of the converter is twice the RMS value which results in higher loss, increased cost and power rating limited.

Reference [10] compared the power conversion for both DCM and BCM, pointing out that, for same converter, power density for DCM is far below that for BCM. However, our studies find that, given same minimum switching frequency, there is no theoretical difference for power density between DCM and BCM, but there is significant difference in conversion efficiency. In DCM, free oscillation after the magnetizing and the demagnetizing period dissipates the energy stored in leak inductance. Whereas in BCM, next magnetizing pulse follows immediately after the first half cycle of the resonant, which means that the leak inductance energy is "wheeled" back to DC bus and at the same time drain voltage of the main switch is clamped to zero to achieve ZVS turn-on. Common to both DCM and BCM, a half cycle resonant is to be inserted prior to the coming magnetizing period, paving the way for ZVS turn on. To minimize the impact on converter power rating, it is desirable to minimize the resonant cycle. In the case that DSP can provide high resolution timing, parasitic capacitor itself is sufficient for that purpose; however, a parallel connected extra capacitor is the common practice in the case that a budget DSP is employed.

As is known, the "transductor" in flyback converter serves both as a transformer and an inductor. Due to the high secondary/primary voltage ratio, which equivalently means high secondary/primary winding ratio, and due to the high switching frequency inherent from high power density and small current ripple, the primary inductance is very small and therefore the leak inductance is of relatively high percentage, yielding in significant percentage leak inductance energy. To

978-1-4244-5046-6/10/$26.00 ©2010 IEEE

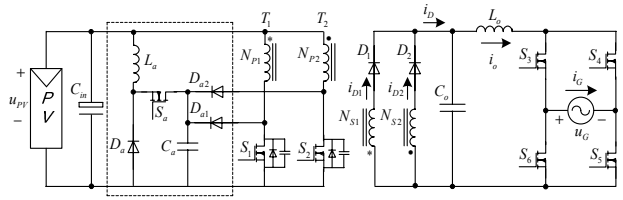

Figure 1. Topology of the grid-connected PV inverter based on soft-switching interleaved flyback converter.

achieve high efficiency and high reliability, the leak inductance energy must be recovered and drain voltage must be clamped.

A grid-connected inverter based on soft-switching interleaved flyback converter is proposed in this paper. Constraint by the optimal power/efficiency ratio, each converter is limited to 100W class, with peak output of 200W. The topology is specially tailored for module integrated or module add-on applications, i.e., one inverter for each PV module. In the proposed topology, all flyback converters share the same leak inductance energy recovery (LIER) circuit which recovers the leak inductance energy in a more efficient way. In this paper, the analysis is based on a two-phase interleaved flyback converter shown as Fig. 1.

II. TOPOLOGY AND CONTROL

A. Topology

Fig. 1 shows the schematic diagram of the proposed single phase grid-connected PV inverter based on soft switching two-phase interleaved soft switching flyback converter. The invert comprises of two-phase interleaved flyback converters, polarity changing circuit and LIER circuit. S_1&S_2 are the main switch of the flyback converters, D_1&D_2 are the output diodes for the respective flyback converters, N_{P1}&N_{P2} are the primary windings and N_{S1}&N_{S2} are the secondary windings. S_3~S_6 form the polarity changing circuit, in which S_3&S_5 turn on during positive half grid cycle, and S_4&S_6 turn on during negative half grid cycle. Together with a buck-type chopper (S_a, L_a and D_a), D_{a1} and D_{a2} form the LIER circuit. The leak inductance energy from T_1 and T_2 is clamped by C_a through D_{a1} and D_{a2} respectively. The buck-type chopper recovers the energy stored in C_a back to C_{in} and at the same time controls the voltage over C_a to form an envelope curve equivalent to the sum of primary voltage and the reflected secondary voltage.

B. Control principles

As shown in Fig. 1, the topology is composed of three parts. The flyback converts and the polarity changing circuit form the frame of the inverter and are controlled coordinately; the LIER circuit on the other hand, is controlled separately and independently.

1) Control of the inverter

For two-phase interleaved flyback converters, each converter is phase-shifted 180° for each switching cycle to achieve equivalent doubled switching frequency and so to reduce current ripple. To ensure BCM at variable instantaneous power, variable switching frequency is essential. Duty cycle is basically determined by input voltage and reflected output voltage, i.e. the grid voltage and transformer winding ratio. Switching on-time is determined by the instantaneous power output. Combining the duty cycle and on-time, switching duty is determined. The envelope curve of the output current is pulsed dc, and converted to grid synchronized sinusoidal form both in phase and amplitude after unfolding through *S3-S6*. S_3(S_5) and S_4(S_6) works in complementary mode at grid frequency, i.e. S_3(S_5) is on when line voltage is positive to neutral and vice versa. As the inverter delivers unity power factor to the grid, S_3~S_6 switch only at zero-voltage-crossing, which is in pace with zero-current-crossing, resulting in both ZVS and ZCS with minimum switching loss. Fig. 2 shows the principle waveforms of the inverter.

2) Control of the LIER circuit

The LIER circuit recovers the leak inductance energy and at the same time controlling the voltage over C_a to follow a voltage trajectory equivalent to the sum of primary voltage and the reflected secondary voltage. The circuit is independently to the main inverter circuit and can be controlled separately with various control strategies, for example, variable switching frequency with fixed on-time/variable off-time, or fixed off-time/variable on-time; or fixed switching frequency. Fig.3 is based on fixed switching frequency. A conventional PI controller is employed to transform the output error to control value, which in turn is compared to triangle pulse train to form the switching signal to force u_{Ca} to follow $u_{PV}+u_G/N$. In Fig.3, $N=N_{S1}:N_{P1}=N_{S2}:N_{P2}$, u_{GSa} is the driving signal for S_a.

III. BCM AND RESONANT SOFT SWITCHING

A. BCM analysis

Let the output voltage of PV array be u_{PV}, for unity power

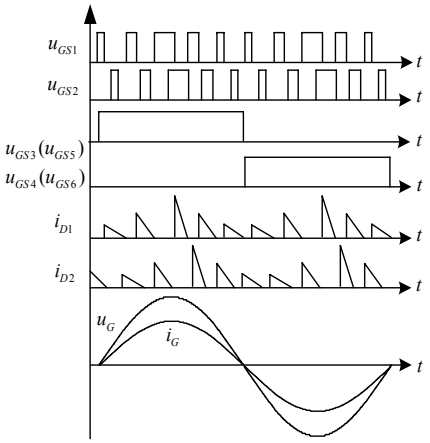

Figure 2. Principle waveforms of the inverter.

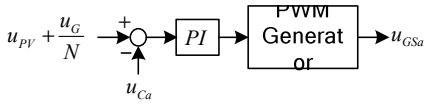

Figure 3. Block diagram of the LIER controller.

factor we have the following instantaneous power:

$$p_o = P_{op} \cdot \sin^2 \omega_G t \tag{1}$$

P_{op} is the peak output power, ω_G is the grid voltage angular frequency.

$$P_{op} = U_{Gp} \cdot I_{op} \tag{2}$$

U_{Gp} and I_{op} are the peak values of the grid voltage and feed-in current.

To achieve BCM operation, two conditions must be satisfied: 1) the sum of magnetizing time and de-magnetizing time equals to the switching cycle *Ts*; 2) the average power in a switching cycle equals to the instantaneous value derived from (1).

$$P_{av} = \int_0^{T_S} p_o dt \tag{3}$$

Let d be the duty cycle of main switch. The first condition introduces the following equation:

$$d \cdot T_S \cdot u_{PV} = \frac{u_G}{N} \cdot (1-d) \cdot T_S \tag{4}$$

Solving (4), we get duty cycle:

$$d = \frac{\frac{u_G}{N}}{u_{PV} + \frac{u_G}{N}} = \frac{u_G}{N \cdot u_{PV} + u_G} \tag{5}$$

For two interleaved converters, each converter delivers half of the total power. The second condition introduces the following equation:

$$\frac{1}{2} L_p \cdot {i_{Sp}}^2 = \frac{P_{op}}{2} \cdot \sin^2 \omega_G t \cdot T_S \tag{6}$$

Where, L_p is the primary inductance and i_{Sp} the primary current peak value.

$$i_{Sp} = \frac{u_{PV}}{L_p} \cdot d \cdot T_S \tag{7}$$

Solving (6) and (7), we get switching cycle:

$$T_S = L_p \cdot P_{op} \cdot \left(\frac{\sin \omega_G t}{u_{PV} d}\right)^2 \tag{8}$$

Based on instantaneous values of PV voltage, grid voltage, peak feed-in power, and the current grid voltage angle, BCM satisfying *Ts* and d are derived from (5) and (8).

B. *Analysis of resonant soft swithching*

The clamping voltage over the drain-source of the main switch is removed after the secondary current reaches zero. With the main switch remaining in off-state, free oscillation begins with primary inductance *Lp* and the equivalent drain-source capacitor *Cs* as the *LC* components Fig. 4 shows the equivalent circuit and main waveform, with the resonant cycle *Tr* determined by:

$$T_r = \frac{2\pi}{\sqrt{L_p C_S}} \tag{9}$$

The drain-source voltage reaches its minimum value after Tr/2, u_{DSmin}=max(u_{PV}-u_G/N, 0). The drain-source voltage can reach zero if $u_G/N > u_{PV}$, making ZVS possible. The resonance is no longer satisfied after drain-source voltage having reached zero and being clamped to zero. After that, the primary current continues to decline but in a linear ratio:

$$\frac{di_{Lp}}{dt} = \frac{u_{PV}}{L_p} \tag{10}$$

Due to the good linearity of sinusoidal curve near zero-crossing, the voltage zero-reaching time for linear declining and resonant does not make much difference. Besides, the

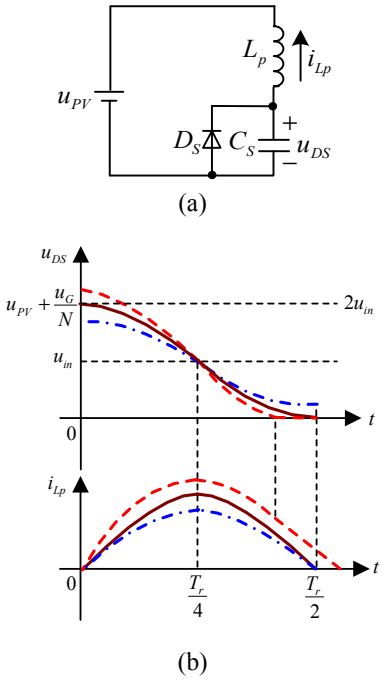

Figure 4. Equivalent resonant circuit and its main waveforms: (a) equivalent circuit, (b) main waveforms.

linear declining rate is less than the resonant rate, in another word, the intersection point of the tangent line with time coordinate is to the right of the intersection point of sinusoidal curve with the time coordinate. That is to say, if $u_G/N > u_{PV}$ and main switch turning-on is delayed $Tr/2$ after demagnetizing, ZVS turn-on is guaranteed.

C. Compensation of leakage inductance and resonant time

The influence of leakage inductance and resonant time on calculating switching cycle and duty cycle is not considered in (5) and (8). As the leakage inductance contributes to a remarkable portion of the primary inductance, its impact on output power and current wave form is not negligible. On the other hand, resonant cycle Tr is the outcome of overall considerations. Under certain conditions, it is often not negligible either. In-depth analysis is given below.

Assume L_p is primary inductance, L_m is primary magnetizing inductance and L_s is primary leakage inductance, we have $L_p = L_m + L_s$. And further more, we have:

$$\frac{1}{2} L_m \cdot i_{Sp}{}^2 = \frac{P_{op}}{2} \cdot \sin^2(\omega_G t) \cdot T_S \tag{11}$$

Combining (5), (7) and (11), we have the modified switching cycle Ts with leak inductance being taken into consideration and resonant cycle being neglected:

$$\begin{aligned} T_S &= \frac{P_{op}}{L_m}[\frac{L_p \cdot (\sin \omega_G t)}{u_{PV} d}]^2 \\ &= \frac{P_{op}}{L_m}\{\frac{L_p \cdot [N \cdot u_{PV} + U_{Gpk} \cdot (\sin \omega_G \cdot t)]}{u_{PV} \cdot U_{Gpk}}\}^2 \end{aligned} \tag{12}$$

Where, U_{Gpk} is the peak value of grid voltage, i.e. $u_G = U_{Gpk}\sin(\omega_G t)$. Therefore the on-time of the main switch with the impact of leak inductance is:

$$\begin{aligned} T_{on} &= d \cdot T_S \\ &= \frac{u_G}{N \cdot u_{PV} + u_G} \cdot \frac{P_{op}}{L_m} \cdot \{\frac{L_p \cdot [N \cdot u_{PV} + U_{Gpk} \cdot (\sin \omega_G \cdot t)]}{u_{PV} \cdot U_{Gpk}}\}^2 \end{aligned} \tag{13}$$

As is known from previous text, a fixed value time piece Tr/2 is inserted before turn-on of the main switch, leading to the actual power output being $(T_S \cdot p_o)/(T_S + T_r/2)$. Obviously, the introduced error is non-linear.

Let's begin from (7) and (11). With Tr being taken into account, let the new turn-on time during the modified switching cycle be $T_{on} = dTm - x$, where $Tm = Ts + Tr/2$, then we have:

$$\begin{aligned} i_{Sp} &= \frac{u_{PV} \cdot (d \cdot T_m - x)}{L_p} \\ \frac{1}{2} \cdot L_m \cdot i_{Sp}^2 &= \frac{P_{op}}{2} \cdot \sin^2(\omega t) \cdot T_m \end{aligned} \tag{14}$$

Solving (14), we have:

$$d^2 \cdot T_m - 2 \cdot d \cdot x + \frac{x^2}{T_m} = \frac{P_{op}}{L_m} (\frac{L_p \sin \omega t}{u_{PV}})^2 \tag{15}$$

Ignoring $\frac{x^2}{T_m}$ as $x << Tm$, we have:

$$T_m = \frac{P_{op}}{L_m}[\frac{L_p \cdot (\sin \omega_G t)}{u_{PV} d}]^2 + \frac{2x}{d} = T_S + \frac{T_r}{2} \tag{16}$$

Then we have: $x = \frac{T_r \cdot d}{4}$, leading to:

$$T_{ON} = d \cdot T_m - x = d \cdot (T_s + \frac{T_r}{2}) - \frac{T_r \cdot d}{4} = d \cdot T_s + \frac{T_r \cdot d}{4} \tag{17}$$

With compensation of leakage inductance and resonant time, the switching cycle Tm is determined by (16), in which Ts is determined by (12); and the switching on-time is determined by (17).

IV. Design Consideration

A. Design of transformer turn ratio

From (5) and (10), the turn ratio of transformer is reflected in the maximum duty cycle of the main switch and influences the ZVS voltage range of the main switch. The higher the turn ratio is, the smaller the maximum duty cycle is, and the smaller the ZVS achievable grid voltage range is. Correspondingly, the smaller the turn ratio is, the higher the reflected grid voltage on the drain-source is, requiring higher voltage tolerance and higher conduction impedance. Therefore, the transformer turn ratio is a compromise amongst maximum duty cycle, ZVS achievable grid voltage range, and choice of the main switch.

B. Switching frequency and primary inductance design

Equation (8) shows that, under BCM condition, the switching cycle of the main switch is related to the instantaneous grid voltage. The higher the instantaneous grid voltage is, the smaller the switching cycle is, i.e. the higher switching frequency is. However, there is always a practical upper limit for switching frequency and therefore BCM is limited to a certain range of the grid voltage. The maximum switching frequency corresponds to the lowest grid voltage.

It is suggested that a preliminary estimation of primary inductance is derived from equation (8); after that verification is conducted through (12) and (16) to ensure a reasonable maximum/minimum switching frequency.

C. Selection of input and output capacitance

The input capacitor is employed to suppress the PV voltage fluctuation during one power cycle, as that will lead to loss in

total yielding energy due to its failure to main at the MPP. With the low frequency character of output power, the input capacitor must be large enough to decouple the pulsed output power and the relatively constant input power. The output capacitor is to filter the high frequency current and to extract its envelope curve for feeding into the utility grid. Apart from eliminating current ripple, the existence of the output capacitor does introduce passive power component, which completes both aspects of pros and cons of the output capacitor and must be taken into good consideration.

V. EXPERIMENTAL RESULTS

An experimental prototype is designed with the following parameters: power rating 200VA, input voltage 30VDC, output voltage 220VAC, switching frequency 150kHz-450kHz, transformer primary/secondary winding ratio 1:6, primary magnetizing inductance 6uH, primary leak inductance 0.6uH, primary main switch FDB2532, resonant capacitor 0.22nF, secondary phase-changing switch 17N80, secondary rectifying diode R8120S3S, output filtering capacitor 0.33uF, output inductance 600uH.

The feed-in current (output current of the inverter) and grid voltage is shown as Fig. 5(a), and the drain to source voltage and drive voltage of the primary switch is shown as Fig. 5(b) and (c). The experimental results show that the utility power factor of the grid-connected inverter is achieved and with the proposed BCM resonant soft switching scheme, the ZVS of the main switch is achieved. It can be seen from Fig. 5(b) that the LIER circuit is effective to clamp the drain to source voltage of main switch following the sum of input voltage and reflected grid voltage. The tested efficiency with output power is shown as Fig. 6, the efficiency at rated output power is 90%. And

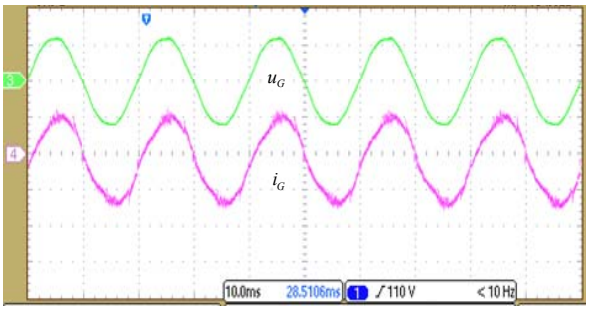

$t:10ms/div$ $u_G:250V/div$ $i_o:1A/div$

(a)

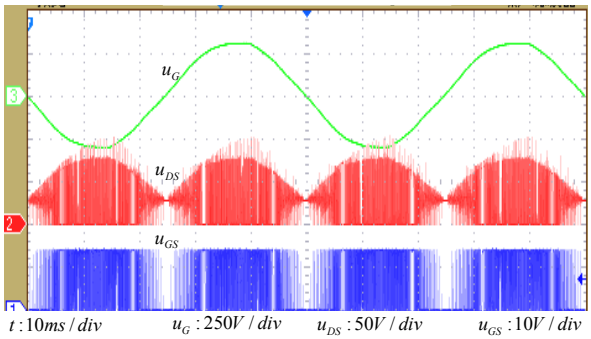

$t:10ms/div$ $u_G:250V/div$ $u_{DS}:50V/div$ $u_{GS}:10V/div$

(b)

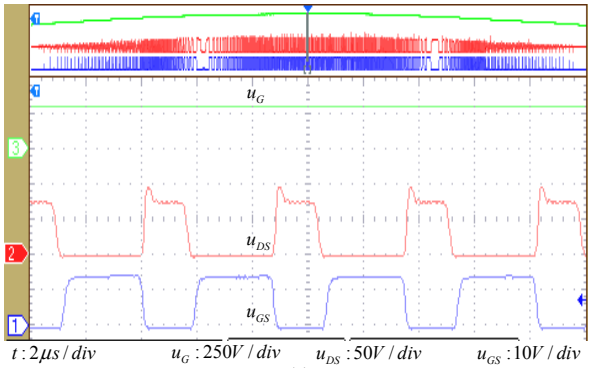

$t:2\mu s/div$ $u_G:250V/div$ $u_{DS}:50V/div$ $u_{GS}:10V/div$

(c)

Figure 5. Experimental results, (a) io and uG, (b) uG, uDS and uGS, (c) expand of (b).

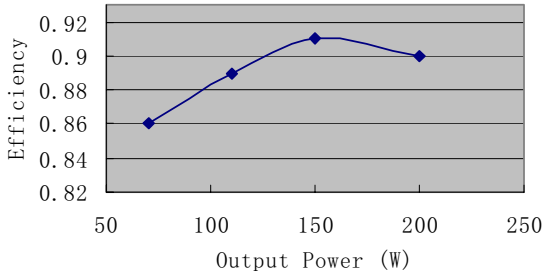

Figure 6. Curve of efficiency vs output power.

Figure 7. Picture of prototype.

finally, the picture of prototype is given in Fig. 7.

VI. CONCLUSION

Through theoretical analysis and experimental results, the proposed interleaved soft switching grid-connected flyback inverter exhibits good character of galvanic isolation at high frequency, single-stage power conversion, high efficiency, high reliability, and robust control. With help of the leak inductance energy recovery circuit, the leak inductance energy is recovered; and with the same circuit, active clamping is achieved paving the way for resonant ZVS turn-on of the main switch. It is therefore possible to use flyback converters to form a higher power rating inverter for higher power rating

applications, as the N interleaved converters share the same leak inductance energy recovery circuit.

REFERENCES

[1] S. B. Kjaer, J. K. Pedersen, and F. Blaabjerg, "Power inverter topologies for photovoltaic modules - a review," in Proc. IEEE IAS Annu. Meeting, 2002, vol.2, pp. 782-788.

[2] P. D. Maycock, "Cost reduction in PV manufacturing: impact on grid-connected and building integrated market," Solar Energy Mater. Solar Cells, vol. 47, no. 1-4, pp. 37-45, Oct. 1997.

[3] Daolian Chen, Jian Liu, "The uni-polarity phase-shifted controlled voltage mode AC-AC converters with high frequency AC link," IEEE Tran. On Power Electronics, vol. 21, no. 4, pp. 889-905, Jul. 2006.

[4] N. P. Papanikolaou, E. C. Tatakis, A. Critsis, and D. Klimis, "Simplified high frequency converter in decentralized grid-connected PV systems: a novel low-cost solution," in Proc. EPE'03, 2003, CD-ROM.

[5] T. Shimizu, K. Wada, and N. Nakamura, "A flyback-type single phase utility interactive inverter with low-frequency ripple current reduction on the DC input for an AC photovoltaic module system," in Proc. IEEE PESC'02, vol. 3, 2002, pp. 1483-1488.

[6] S. B. Kjaer and F. Blaabjerg, "Design optimization of a single phase inverter for photovoltaic applications," in Proc. IEEE PESC'03, vol. 3, 2003, pp. 1183-1190.

[7] S. Mekhilef, N. A. Rahim, and A. M. Omar, "A new solar energy conversion scheme implemented using grid-tied single phase inverter," in Proc. IEEE TENCON'00, vol. 3, 2000, pp. 524-527.

[8] D. C. Martins and R. Demonti, "Grid connected PV system using two energy processing stages," in Conf. Rec. 29th IEEE Photovoltaic Specialists Conf., 2002, pp. 1649-1652.

[9] S. B. Kjaer, J. K. Pedersen, F. B. Blaabjerg, "A review of single-phase grid-connected inverters for photovoltaic modules," IEEE Tran. On Industry Applicatios, vol. 41, no. 5, pp.1292-1306, Sep/Oct. 2005.

[10] A. C. Kyritsis, N. P. Papanikolaou, E. C. Tatakis and J. C. Kobougias, "Design and control of a current source flyback inverter for decentralized grid-connected photovoltaic systems," in Conf. Power Electonics and applications, European, 2005, pp. 1-10.

[11] A. C. Kyritsis, E. C. Tatakis and N. P. Papanikolaou, "Optimum design of the current –source flyback inverter for decentralized grid-connected photovoltaic systems," IEEE Tran. On Energy Conversion, vol. 23, no. 1, pp.281-193, Mar. 2008.

[12] Toshihisa Shimizu, Keiji Wada, Naoki Nakamura, "Flyback-type single-phase utility interactive inverter with power pulsation decoupling on the DC input for an AC photovoltaic module system," IEEE Transactions On Power Electronics, vol. 21, no. 5, pp. 1264-1272, Sep. 2006.